Equal parallel and cone-beam projections: a curious property of D-symmetric object functions

Rolf Clackdoyle, Simon Rit

Equal parallel and cone-beam projections: a curious property of D-symmetric object functions

Rolf Clackdoyle[1] and Simon Rit[2]

[1] Univ. Grenoble Alpes, CNRS, Grenoble INP, TIMC-IMAG
Pavillon Taillefer, 38706 La Tronche, Grenoble, France

[2] Univ. Lyon, INSA-Lyon, UCB Lyon 1, UJM-Saint Etienne, CNRS, Inserm,
CREATIS UMR5220, U1294, F-69373 Lyon, France

Corresponding author email: rolf.clackdoyle@univ-grenoble-alpes.fr

Short Title: D-symmetric objects have equal parallel and divergent projections

June 9, 2023

Abstract

In tomographic image reconstruction, the object density function is the unknown quantity whose projections are measured by the scanner. In the three-dimensional (3D) case, we define the D-reflection of such a density function as the object obtained by a particular weighted reflection about the plane $z = D$, and a D-symmetric function as one whose D-reflection is equal to itself. D-symmetric object functions have the curious property that their parallel projection onto the detector plane $z = D$ is equal to their cone-beam projection onto the same detector with x-ray source location at the origin. Much more remarkable is the additional fact that for any fixed D-symmetric object, *every* oblique parallel projection onto this same detector plane equals the cone-beam projection for a corresponding source location. The mathematical proof is straight forward but not particularly enlightening, and we also provide here an alternative physical demonstration that explains the various weighting terms in the context of classical tomosynthesis. Furthermore, we clarify the distinction between the new formulation presented here, and the original formulation of Edholm and co-workers who obtained similar properties but for a pair of objects whose divergent and parallel projections matched, but with no D-symmetry. We do not claim any immediate imaging application or useful physics from these notions, but we briefly comment on consequences for methods that apply data consistency conditions in image reconstruction.

1 Introduction

In the context of image reconstruction from projections, the theoretical principles for the parallel-projection case are much simpler and more readily understood than those for divergent projections. A theorem linking these two domains was presented in the mid-1990s by Edholm and co-workers (Carlsson *et al* 1994, Edholm and Danielsson 1996, and Edholm and Danielsson 1998). They announced the surprising fact that, in a tomosynthesis geometry with x-ray sources lying in a plane, all the cone-beam projections of a 3D object density function are equal to corresponding parallel-beam projections of a second 'hypothetical' 3D object density function. This Edholm and Danielsson (ED) theorem opened the door to the possibility of processing divergent projection data as if they were parallel, and, if needed, subsequently converting the hypothetical object back to its corresponding divergent-beam object. In spite of their comment "it is unlikely that [the theorem] will provide us with fundamentally new insights in 3D-reconstruction from cone-beam data" (Edholm and Danielsson 1996), the result has indeed generated both clarity and new insights in cone-beam and fan-beam tomography, as well as a variety of imaging applications.

An early application was described by Carlsson *et al* (1994) whereby an unmeasured cone-beam projection was generated directly from measured projections in a circular tomosynthesis geometry, by appealing to parallel-beam theory and applying Fourier transforms. Patch (2002) also pointed out this approach to generating unmeasured projections in the circular tomosynthesis geometry, although she used a different method involving John's equation (John, 1938) in her implementation (Patch, 2000).

Image reconstruction applications of the ED theorem appeared in 2007. Nett *et al* (2007) used the ED theorem as a direct method of image reconstruction for circular tomosynthesis. By considering all the measured projections as parallel, they could use a simple ramp-filtering approach (albeit with a missing region in 3D Fourier space) to reconstruct the hypothetical object (which they called a 'virtual' object), but rather than creating it explicitly and converting to the divergent ('true') object, they directly performed the conversion at backprojection time, to reconstruct the desired object. Along similar lines, but going much further, Zhu *et al* (2007) considered a conventional circular cone-beam geometry (with the detector not parallel, but perpendicular to the source plane), mathematically converted to a parallel (tomosynthesis) geometry, used ramp-filtering, and then mathematically converted the 'hypothetical' object to the correct reconstructed image. Most importantly, this reconstruction procedure was shown to be mathematically identical to the well-known FDK routine (Feldkamp *et al*, 1984) and therefore provided an independent justification to that of Defrise and Clack (1994) for the FDK procedure. Zhu *et al* went further, and applied the same approach for shortscan circular cone-beam data, again used the elementary parallel-beam theory, and derived a novel cone-beam shortscan algorithm.

The ED theorem also led to a number of advances in so-called Data Consistency Conditions (DCC). Over the last 10 years, Clackdoyle and co-workers published several results on divergent beam DCC. If a set of parallel projections satisfy their DCC, then they correspond to an underlying object function. But the same projections will also correspond to an underlying hypothetical object and hence the same DCC for the parallel projections must also apply to divergent projections. DCC were thus established for fan-beam projections on a line (Clackdoyle, 2013), for cone-beam projections on a plane (Clackdoyle and Desbat, 2013), and divergent projections in

linogram or planogram format (Clackdoyle, 2018). The existence of high-order moment conditions that appeared in the fan-beam case led to the development of DCC for truncated parallel and fan-beam projections (Clackdoyle and Desbat, 2015) and for fan-beam projections on small arc of a circle (Clackdoyle *et al*, 2015). All these DCC have been further exploited for applications such as patient motion detection (Clackdoyle *et al*, 2014; Clackdoyle and Desbat, 2015; Boulier *et al*, 2018), parameter estimation (Clackdoyle *et al*, 2015); and geometric calibration (Lesaint *et al*, 2017; Desbat and Clackdoyle, 2019; Nguyen *et al*, 2020).

It is fair to say that the ED theorem has had theoretical benefits, and has also facilitated various medical imaging applications.

In this work, we further develop the ED theorem, and show that it is possible for both the original (divergent beam) object and the hypothetical (parallel-beam) object to actually coincide, and still maintain the same property of matched divergent and parallel projections. In other words, there exist objects whose parallel projections are the same as their divergent projections. This surprising result arises in a slightly different geometric formulation of the 'tomosynthesis geometry' where the locations of the detector and the source plane are inverted. The original ED theorem also applies in this alternative formulation, but the existence of objects with matched projections does not occur in the original formulation. We discuss these points in detail in section 4.

In section 2 below, we present the theory and mathematical demonstrations. We first establish the coordinate system of our geometric formulation, and establish the notation for divergent and parallel projections. We then define the notions of D-reflection and D-symmetry of object functions. Next, we demonstrate the key link between D-reflections and divergent and parallel projections: the D-reflection of a "divergent" object turns out to be the corresponding parallel (or hypothetical) object. The main result then follows immediately: that a D-symmetric object will be simultaneously a divergent object and its parallel counterpart. In section 3, we provide an independent, more enlightening, physics-style demonstration that operation of D-reflection does convert divergent objects to parallel objects. This demonstration is in the context of the tomosynthesis geometry and carefully explains the individual terms of the definition of D-symmetry. In section 4, we explain the differences between the Edholm formulation and our formulation, and we pinpoint why the Edholm formulation does not also generate D-symmetry and objects with matched divergent and parallel projections. We also provide more illustrations of D-symmetric objects and we discuss the potential significance of the D-symmetric concept. We end with a brief summary of the main points presented in this paper.

All the results given here apply in an obvious way in any dimension (greater than one-dimension). For clarity, the mathematical and physical presentations are given explicitly for the 3D case, and after figure 1, all the illustrations are given in two-dimensions.

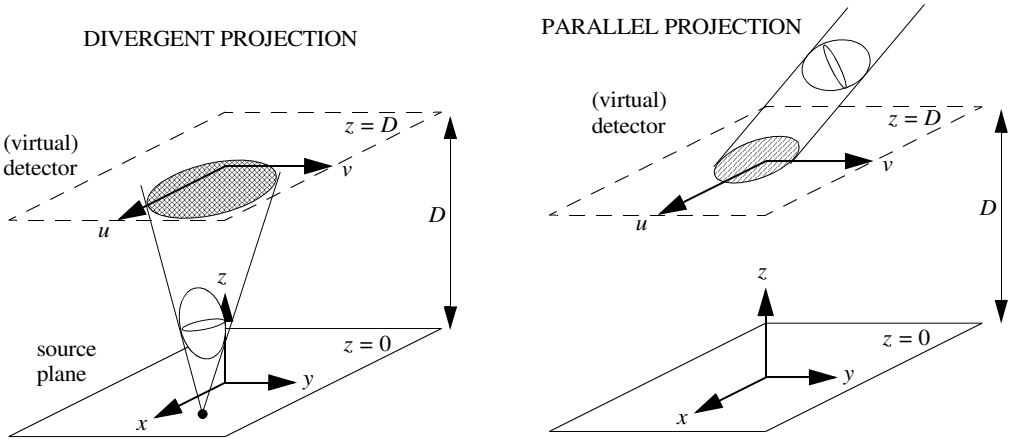

Figure 1: Illustration of the geometry. Left: divergent beam (cone-beam or fanbeam) sources lie on the $z = 0$ plane, and the virtual detector lies at $z = D$. Right: a parallel projection onto the virtual detector. Note that for both projections, the object can be either side of the detector and can intersect the detector. Figures 3 (top) and 11 illustrate objects that straddle the virtual detector.

2 D-symmetry and matched projections

2.1 Cone-beam and parallel projections

Throughout this paper, we assume a fixed positive value of D which is the distance from the detector plane to the origin. The detector is parallel to the x-y plane. All objects are assumed to be of finite size and lie above the x-y plane; mathematically, all object functions have compact support which lies between the planes $z = \varepsilon$ and $z = D^2/\varepsilon$ for some small fixed ε (and certainly $\varepsilon < D$). The detector plane $z = D$ is considered a *virtual* detector to allow the possibility that the object intersects the detector plane. The detector has (u, v) coordinates that are aligned in the (x, y) directions. Figure 1 illustrates the geometry with an example cone-beam projection and an example parallel projection.

For cone-beam projections, we consider a so-called source position $s \in \mathbb{R}^3$ which will always be on the x-y plane, so $s = (s_x, s_y, 0)$. To simplify some of the notation, we also define $d_{u,v} = (u, v, D)$ to be the 3D point at the (u, v) location on the detector. Now we can define the (cosine-weighted) cone-beam projection of f with the source at position s, by

$$\mathcal{D}_s f(u, v) = \frac{D}{||d_{u,v} - s||} \int_0^\infty f\left(s + t\frac{d_{u,v} - s}{||d_{u,v} - s||}\right) dt \tag{1}$$

which is the standard definition of a cone-beam projection except for the leading term $D/||d_{u,v} - s||$.

Note that the smallest possible value of $||d_{u,v} - s||$ is D which occurs for $d_{u,v}$ directly above s, i.e. $(u, v) = (s_x, s_y)$. In this case, the ray from s to $d_{u,v}$ strikes the detector perpendicularly, which we refer to as zero angle-of-incidence. For rays that strike obliquely, the cosine of the incidence angle will be $D/||d_{u,v} - s||$, which explains the terminology for this leading term. A change of integration variables in equation (1), replacing t with $z||d_{u,v} - s||/D$, provides a simpler expression where the cosine term is hidden inside the integral:

$$\mathcal{D}_S f(u, v) = \int_0^\infty f\left(s_x + \frac{z}{D}(u - s_x),\ s_y + \frac{z}{D}(v - s_y),\ z\right)\, dz. \tag{2}$$

The (cosine-weighted) parallel projection of f, in the direction $\theta = (\theta_x, \theta_y, \theta_z) \in S^2$ is given by

$$\mathcal{P}_\theta f(u, v) = |\theta_z| \int_{-\infty}^\infty f\left(d_{u,v} + t\theta\right)\, dt = |\theta_z| \int_{-\infty}^\infty f(u + t\theta_x, v + t\theta_y, D + t\theta_z)\, dt \tag{3}$$

and the leading $|\theta_z|$ is again a cosine term. For parallel projections, the sign of the direction vector is irrelevant: $\mathcal{P}_\theta = \mathcal{P}_{-\theta}$. Since $\mathcal{P}_\theta$ is a parallel projection, all rays strike the detector at the same incidence angle, whose cosine is easily seen to be $|\theta_z|/||\theta|| = |\theta_z|$.

When matching up cone-beam and parallel projections, a source location s for the cone-beam projection will correspond to a parallel projection with direction θ_S given by $\theta_S = (s_x, s_y, D)/\sqrt{s_x^2 + s_y^2 + D^2}$. Now, applying θ_S in equation (3), and changing variables $t = (z - D)\sqrt{s_x^2 + s_y^2 + D^2}/D$, we obtain

$$\mathcal{P}_{\theta_s} f(u, v) = \int_{-\infty}^\infty f\left(u - s_x + \frac{z}{D}s_x,\ v - s_y + \frac{z}{D}s_y,\ z\right)\, dz. \tag{4}$$

For the rest of this article, we use the equation (2) and equation (4) versions for the projections $\mathcal{D}_S$ and $\mathcal{P}_{\theta_s}$.

The original Edholm and Danielsson formulation differed from the description above in that their detector was the x-y plane, and the sources lay on the plane $z = D$. Furthermore, a different correspondence between source positions and parallel projection directions was used in their formulation. We discuss these differences and their consequences in section 4 below. The formulation described here was suggested by Defrise (2017).

2.2 D-reflections

Recalling that $f(x, y, z) = 0$ for $z < \varepsilon$, we define the D-reflection of f as

$$\mathcal{T} f(x, y, z) = \begin{cases} \dfrac{D^2}{z^2} f\left(\dfrac{Dx}{z}, \dfrac{Dy}{z}, \dfrac{D^2}{z}\right) & \text{if } z > 0 \\ 0 & \text{if } z \leq 0 \end{cases} \tag{5}$$

and we note from this definition that $f(x, y, z) = 0$ for $z \notin (\varepsilon, D^2/\varepsilon)$ if and only if $\mathcal{T} f(x, y, z) = 0$ for $z \notin (\varepsilon, D^2/\varepsilon)$.

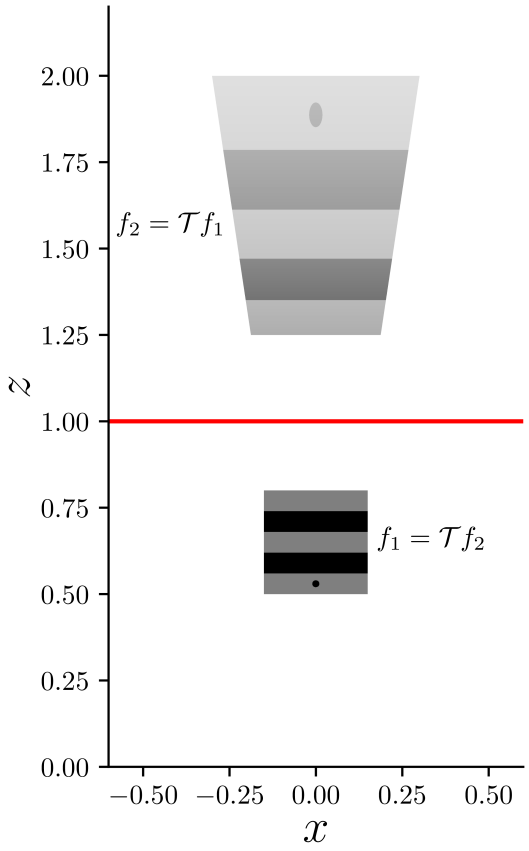

Figure 2: Illustration of D-reflections. The object f_1 lies below the detector (red line) and consists of alternating bands of constant intensity, and a small disk. Its D-reflection, $f_2 = \mathcal{T} f_1$, reveals how these bands are reduced in intensity and are magnified horizontally. These effects are greater with increased distance from the detector. There is also a vertical stretching, which increasingly thickens the bands, and converts the circular disk into an ellipse. The D-reflection of f_2 is $\mathcal{T} f_2 = f_1$.

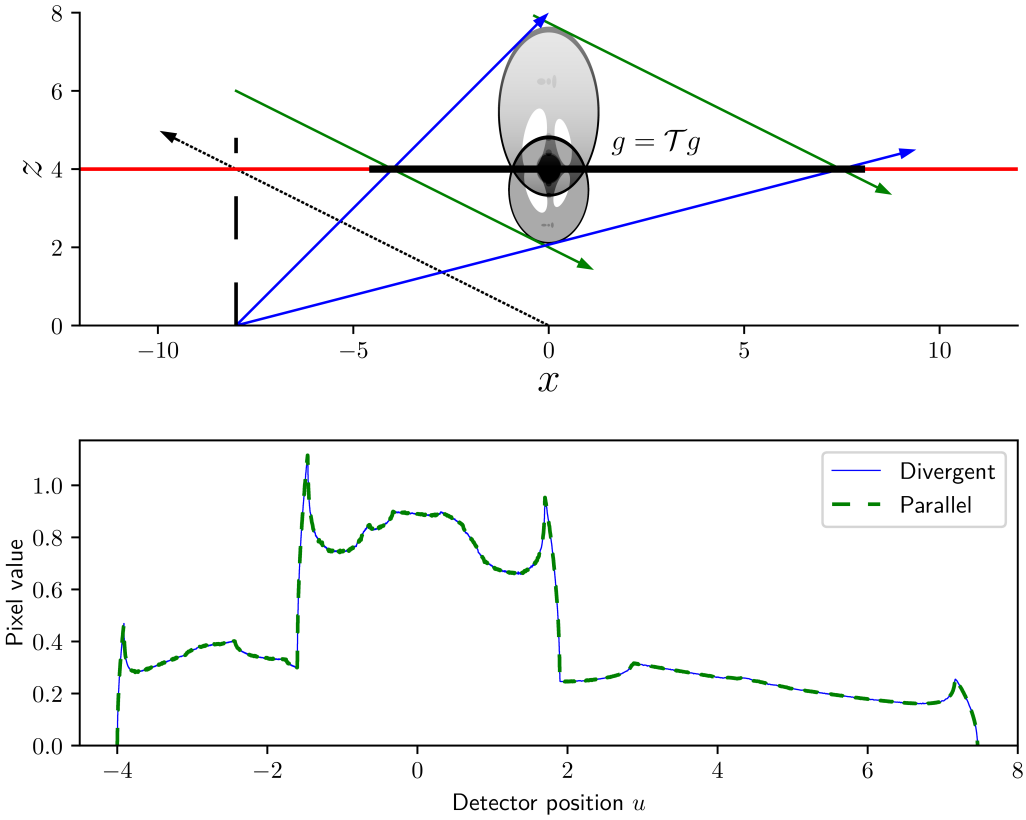

Figure 3: A 2D example of a D-symmetric function, illustrating the matched fan-beam and parallel projections. Above: the red line is the virtual detector, $z = D$ with $D = 4$. The composite object, g, was formed by adding a small translated Shepp-Logan phantom f to its D-reflection $\mathcal{T}f$. Note that the Shepp-Logan phantom f straddled the virtual detector, resulting in an overlapping behavior in g which does not change the validity of the object. The blue lines trace the envelope of the fan-beam projection from the source location $(s_x, 0) = (-8, 0)$ and the green lines outline the parallel projection with direction $(-8, 4)/\sqrt{80}$. Bottom: the two projections match exactly, as shown in the plot. It is surprising that such objects can exist, with a matched pair of fan-beam and parallel projections. Much more remarkable is the fact that for this same fixed object g, for *every* fan-beam location $(s_x, 0)$ and parallel projection direction $(s_x, 4)/\sqrt{s_x^2 + 4^2}$, the two fan-beam and parallel projections match. This property is true for any D-symmetric object g (i.e., for any $g = \mathcal{T}g$).

We call this transform $\mathcal{T}$ a reflection because along the plane $z = D$, the features of f remain unchanged ($\mathcal{T}f(x, y, D) = f(x, y, D)$) and because $\mathcal{T}\mathcal{T}f = f$ (readily seen by writing $\mathcal{T}f = g$ and showing that $\mathcal{T}g = f$ by direct calculation). However, there is some intensity weighting, some magnification effect, and considerable stretching in the z direction, as evidenced by the fact that the region $z \in [\varepsilon, D]$ is mapped (reflected) into the region $z \in [D, D^2/\varepsilon]$ and vice versa. So $\mathcal{T}$ is not a true mirror reflection, but a "distorted reflection". Figure 2 provides an example 2D object, f_1, and its D-reflection $f_2 = \mathcal{T}f_1$, illustrating the intensity weighting, the horizontal magnification effect, and the vertical stretching features.

If an object g is the same as its D-reflection ($g = \mathcal{T}g$), we call it a D-symmetric object. Obviously, any D-symmetric object must have components on both sides of the reflecting plane $z = D$. We note that D-symmetric functions can readily be generated by combining any object with their D-reflection, i.e. $g = f + \mathcal{T}f$ is D-symmetric, so there is a huge abundance of such object density functions.

2.3 Matched projections: $\mathcal{D}_S g = \mathcal{P}_{\theta_s} g$ for D-symmetric objects g

The main result that we are presenting is: if g is a D-symmetric object function, then the divergent projections of g are equal to its parallel projections on the same detector. Mathematically, if $\mathcal{T}g = g$ (D-symmetry), then $\mathcal{D}_S g = \mathcal{P}_{\theta_s} g$ (matched projections) for all source positions s on the $z = 0$ plane. The correspondence between the parallel-beam direction and the source location is given by $\theta_S = (s_x, s_y, D)/\sqrt{s_x^2 + s_y^2 + D^2}$ as was mentioned in section 2.1 above.

The key feature of D-reflections is that they convert (divergent) objects to their hypothetical parallel objects. Specifically, we will show below that the divergent projections of an object f are the same as the parallel projections of its D-reflection, $\mathcal{T}f$. Mathematically, we show that $\mathcal{D}_S f = \mathcal{P}_{\theta_s}\mathcal{T}f$.

It is now immediately obvious that for a D-symmetric object g, the action of D-reflection just returns the same object $\mathcal{T}g = g$, and therefore $\mathcal{D}_S g = \mathcal{P}_{\theta_s} g$. All D-symmetric objects have matched divergent and parallel projections. See figure 3 for an illustration in two-dimensions. (Note that for figures 3, 4, 10, and 11, we used a modified, high-contrast version of the Shepp-Logan phantom (see page 201 of Toft and Sorenson (1996)).)

Here we show the fundamental result that, for all $(s_x, s_y) \in \mathbb{R}^2$, we have $\mathcal{D}_S f = \mathcal{P}_{\theta_s}\mathcal{T}f$ where the object function f satisfies $f(x, y, z) = 0$ for $x \notin (\varepsilon, D^2/\varepsilon)$. Starting with the right-hand-side, applying equation (4) we note that the limits of integration can be changed from $(-\infty, \infty)$ to $(\varepsilon, D^2/\varepsilon)$ because $\mathcal{T}f(x, y, z) = 0$ for $z \notin (\varepsilon, D^2/\varepsilon)$. After using equation (5) to remove $\mathcal{T}$, the crucial step is the change of variables $z' = D^2/z$ so $dz' = (-D^2/z^2)\, dz$:

$$\begin{aligned}
\mathcal{P}_{\theta_s}\mathcal{T}f(u, v) &= \int_{\varepsilon}^{D^2/\varepsilon} (\mathcal{T}f)\left(u - s_x + \frac{z}{D}s_x,\, v - s_y + \frac{z}{D}s_y,\, z\right) dz \\
&= \int_{\varepsilon}^{D^2/\varepsilon} \frac{D^2}{z^2} f\left(\frac{D(u - s_x + (z/D)s_x)}{z}, \frac{D(v - s_y + (z/D)s_y)}{z}, \frac{D^2}{z}\right) dz
\end{aligned}$$

$$
\begin{aligned}
&= -\int_{D^2/\varepsilon}^{\varepsilon} f\left(\frac{D(u-s_x)}{D^2/z'}+s_x,\ \frac{D(v-s_y)}{D^2/z'}+s_y,\ \frac{D^2}{D^2/z'}\right) dz' \\
&= \int_{\varepsilon}^{D^2/\varepsilon} f\left((u-s_x)\frac{z'}{D}+s_x,\ (v-s_y)\frac{z'}{D}+s_y,\ z'\right) dz' \\
&= \mathcal{D}_s f(u,v) \qquad (6)
\end{aligned}
$$

where, in the last line, we can replace the integration limits $(\varepsilon, D^2/\varepsilon)$ with $(0,\infty)$ since $f(x,y,z) = 0$ for $z \notin (\varepsilon, D^2/\varepsilon)$.

Therefore, $\mathcal{D}_S f = \mathcal{P}_{\theta_s}\mathcal{T} f$. Given f_1, if we let $f_2 = \mathcal{T} f_1$ then f_2 is the 'parallel object' corresponding to the 'divergent object' f_1, i.e., the parallel projections of f_2 match the divergent projections of f_1. If we now take f_2 to be the divergent object, then $\mathcal{T} f_2$ is its corresponding parallel object. By the reflecting property of $\mathcal{T}$, we obviously obtain $\mathcal{T} f_2 = \mathcal{T}\mathcal{T} f_1 = f_1$, so the roles of f_1 and f_2 can be reversed. See figure 4 for an example f_1, f_2 pair. In the original Edholm formulation, the reflection property is not present so the roles of f_2 and f_1 cannot be reversed. Similarly, the Edholm formulation does not provide objects g with self-matched divergent and parallel projections.

3 The tomosynthesis model

Although the mathematical demonstration is straight-forward, the underlying mechanisms are not obvious. In this section, we provide a geometric description for why the D-reflecting operator $\mathcal{T}$ provides the 'parallel object' $f_2 = \mathcal{T} f_1$ that corresponds to the 'divergent object' f_1.

An explanation in physical terms of the formula for $\mathcal{T}$ can be based on the well-known principles of focal plane tomography, also known as classical blurring tomography, tomosynthesis, or body section tomography. See, for example, section 3.2 of (Buzug, 2008). Briefly, if an x-ray source is translated in a plane parallel to the detector, the projection of the object moves in a complementary way on the detector. More specifically, each longitudinal slice of the object (slice parallel to the detector), if considered in isolation, will be imaged with its own constant magnification factor, and the projected image of this slice translates at a speed determined by the magnification factor and the speed of the source. The projections of different longitudinal slices thus translate at different speeds. The imaging principle was to translate the detector (x-ray film) to match the movement of the desired longitudinal slice, which would therefore remain focused on the detector while neighboring slices were blurred due to mismatched relative motion.

This principle relies heavily on the detector being oriented parallel to the plane of motion of the x-ray source. The x-ray source can nevertheless be located "at infinity" with respect to the detector and the same principles then apply to parallel projection images.

The idea behind understanding the $\mathcal{T}$ transformation is to decompose the (cone-beam) object f_1 into thin "z-slices" which we index by z_1 and to consider only the effect of one such fixed slice $f_1(x,y,z_1)$, see figure 5 (left). This slice produces an image $I_1(x,y)$ on the $z = D$ detector plane and this image translates in response to translation of the source $s = (s_x, s_y, 0)$. We will construct

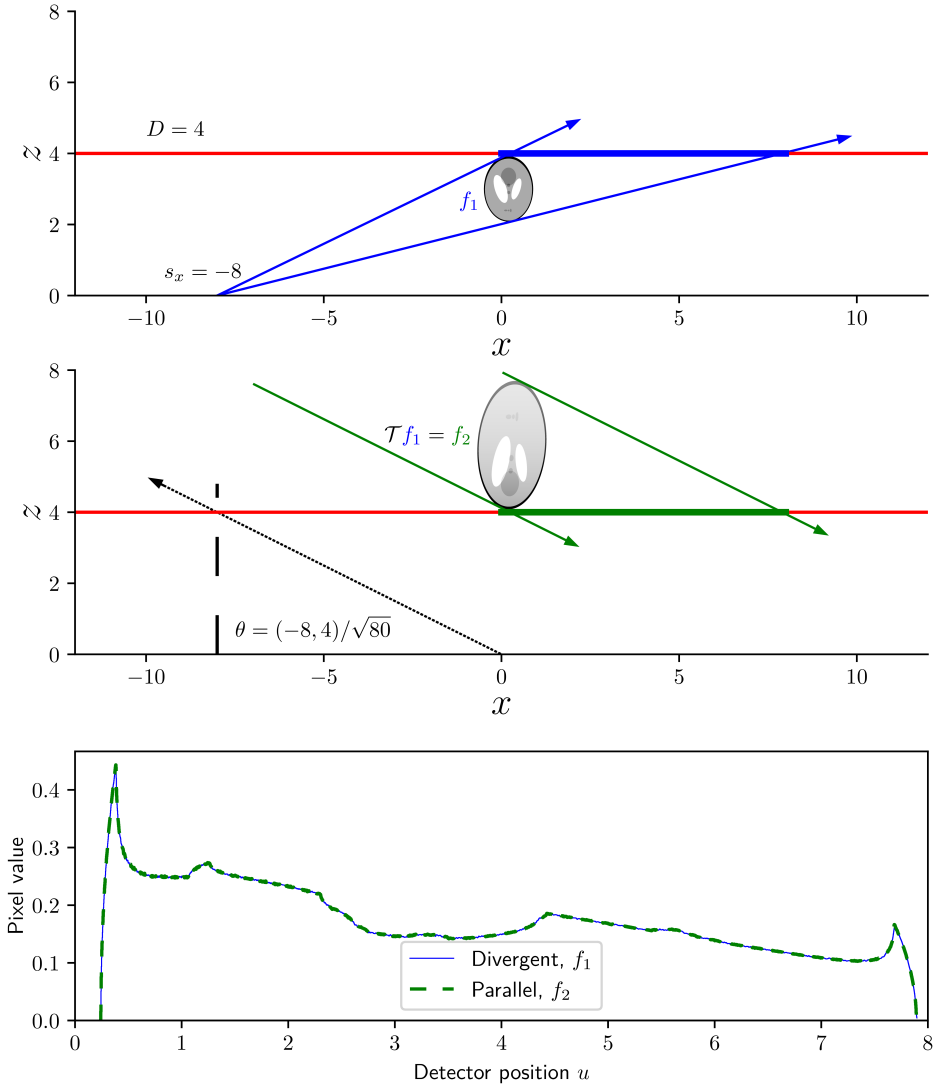

Figure 4: Example 2D objects f_1 and f_2 with matching projections. The fan-beam projection $\mathcal{D}_s f_1$ on the detector plane $y = D$ is indicated by the solid blue horizontal line segment in the top image. The source location is $s = (-8, 0)$ and the detector is at $D = 4$. In the middle image, the object f_2 is shown, with parallel projection $\mathcal{P}_{\theta_s} f_2$ indicated by the green horizontal line segment. The direction of the projection is given by $\theta = (s_x, D)/\sqrt{s_x^2 + D^2}$ (the green arrows point in the $-\theta$ direction). The bottom image shows the plotted projection values for both $\mathcal{D}_s f_1$ and $\mathcal{P}_{\theta_s} f_2$ and they coincide exactly. This single example is not remarkable. However, for this pair f_1, f_2, *all* pairs of projections match, for any s on the x-axis and corresponding direction θ. The object f_2 is obtained from f_1 using the D-reflecting transformation $\mathcal{T}$.

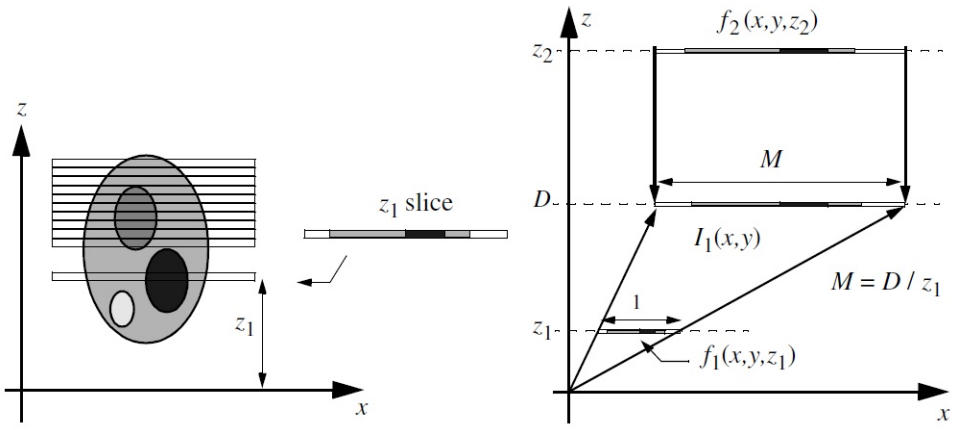

Figure 5: Left: The object f_1 is decomposed into slices perpendicular to the z axis, so thin that for each slice the density function can be considered constant in the z direction. Each slice is identified by its distance to the $z = 0$ plane. Right: From a source positioned at the origin, the cone-beam projection of the z_1-slice $f(x, y, z_1)$ onto the detector at $z = D$ produces an image $I_1(x, y)$ which is the magnification of $f(x, y, z_1)$. The magnification factor is $M = D/z_1$ as can be seen from a simple argument using similar triangles. A z_2 slice from the parallel object f_2 is easily constructed and positioned such that its parallel projection is exactly $I_1(x, y)$.

a corresponding slice $f_2(x, y, z_2)$ of the object f_2 whose parallel image on the detector responds identically to the cone-beam image, when the projection direction θ_s varies.

In building f_2 in this fashion, there will be four physical effects to consider. One is the cosine of the incidence angle; another is the magnification of the cone-beam slice which does not occur for the f_2 slice; a third effect is the distance of the slice from the detector, which will control the speed of translation relative to the speed of translation of the source; and the fourth effect will be a scaling of intensity that depends on the z-direction.

3.1 The magnification factor

We begin with the magnification factor. Fixing for now the source location at the origin, we note that, because it is "thin", the z_1-slice will cast a projection $I_1(x, y)$ whose intensities are the same as those of the z_1-slice, except that $f_1(x, y, z_1)$ will be magnified by the time it reaches the $z = D$ detector. The magnification factor $M(z_1)$ which we write as M for short, is easily seen to be $M = D/z_1$. See figure 5 (right). The relation between the z-slice and its projection, after taking into account the magnification, is therefore $I_1(Mx, My) = f_1(x, y, z_1)$.

Now, since a parallel projection of a z-slice (even an oblique parallel projection) will not undergo any magnification, the parallel-object slice $f_2(x, y, z_2)$ will be the same size as its projection $I_2(x, y)$. We can therefore choose any z_2 and define the z_2-slice as $f_2(x, y, z_2) = I_1(x, y)$. The f_2 z-slice

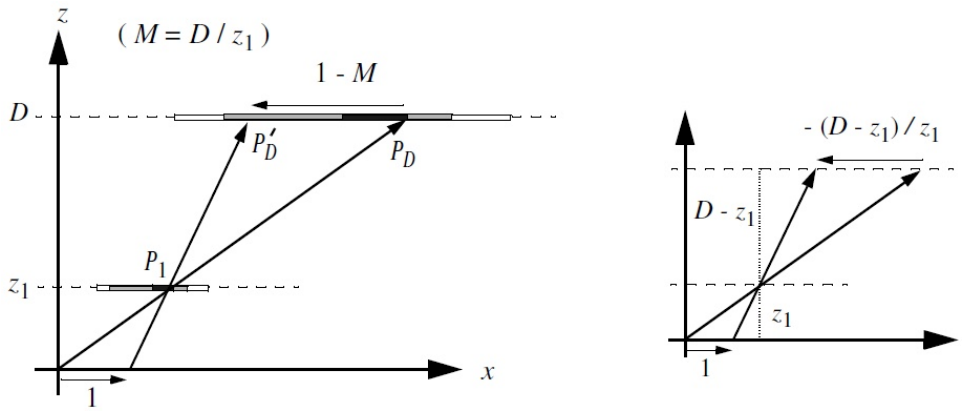

Figure 6: Left: for a stationary z-slice, a movement of the source by a unit distance will result in the cone-beam image of the z-slice to translate on the detector, in the opposite direction, by $1 - M$ units where M is the magnification factor. Any point P_1 on the z-slice will project to P_D with the source at the origin, and to P'_D with the source translated. The distance $P_D - P'_D$ is $1 - M$ as shown at right. Right: A simple application of similar triangles shows that the motion from P_D to P'_D at left is given by $(z_1 - D)/z_1$ which is equal to $1 - M$.

is thus bigger than its corresponding f_1 z-slice due to the magnification of the f_1 slice. The parallel projection $I_2(x, y)$ of the f_2 z-slice taken "from above" ($\theta_S = (0, 1)$) will match the cone-beam projection of the z_1-slice $f_1(x, y, z_1)$, as illustrated in figure 5 (right). Taking into account the magnification (but no other issues), we see the correspondence between z-slices of the two objects is determined by matching the projections $I_1(x, y)$ and $I_2(x, y)$ and therefore given by $f_1(x, y, z_1) = I_1(Mx, My) = f_2(Mx, My, z_2)$ where M depends on the location z_1 of the cone-beam slice f_1 and z_2 is free (for now).

For any contributing slices of the cone-beam object f_1 which lie above the detector, i.e. $z_1 > D$, the magnification factor will be less than 1, the image $I_1(x, y)$ will be smaller than the slice $f_1(x, y, z_1)$, and in this case the corresponding parallel object z_2-slice of f_2 will be smaller than that of f_1.

We will see below that any cone-beam z_1-slice will have its corresponding f_2 object z-slice on the opposite side of the detector, which generates the reflection behavior.

3.2 Matching the translation speeds of the projection images

We now study how the images $I_1(x, y)$ and $I_2(x, y)$ translate in response to movement of the source location and change of angle of parallel projection. First the cone-beam case, $I_1(x, y)$. The location of the z_1-slice relative to the detector and the source determines the speed of translation of the cone-beam image as the source moves. We fix the z_1-slice of f_1 and note that if the source is translated a unit distance to a new location with respect to the origin, the cone-beam image of

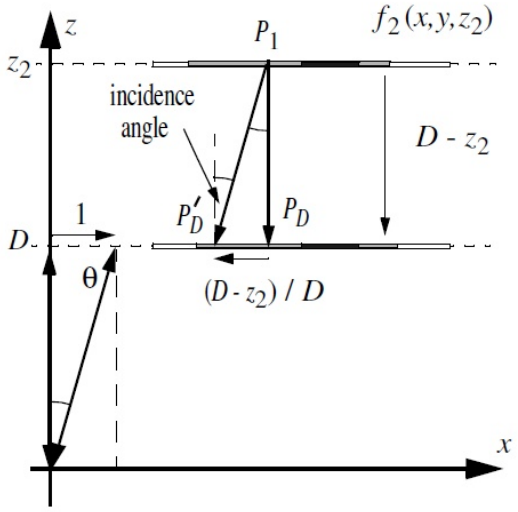

Figure 7: When the direction of projection changes, the parallel projection of a z-slice $f(x, y, z_2)$ will translate across the detector: the projection of any fixed point P_1 on the z-slice is labeled P_D for projection at incidence angle zero ($\theta = (0, 1)$), and moves to P'_D when the angle changes. Specifically, the displacement will be $(D-z_2)/D$ for a change from $\theta = (0, 1)$ to $\theta = (1, D)/\sqrt{1 + D^2}$ as is evident from similar triangles in the figure. Note that the direction of translation is the reverse of the direction of (change of) tangent of the incidence angle.

this z_1-slice will translate by a distance $1 - M$, as shown in figure 6. If the slice lies in front of the detector, ($z_1 < D$) then the image translates in the opposite direction of the source translation, consistent with the negative value of $1 - M$. If the z-slice is behind the detector, the movement of the source and the image is in the same direction, and again by a distance $1 - M$, as can be verified by constructing figures (not shown here) in the same spirit as figure 6.

For parallel projections of a z_2 slice $f_2(x, y, z_2)$, we first note that although there is no magnification effect, there is still a translation of the image $I_2(x, y)$ when the angle of the parallel projection changes. The speed of the translation is proportional to how far the z_2-slice lies from the $z = D$ detector plane. More importantly, for a fixed z_2-slice, when considering a changing projection angle, the displacement is proportional to the change in tangent of the incidence angle with the detector (see figure 7). This fact motivates the definition of the link between θ (direction vector of the parallel projection) and s (the location of the cone-beam source). By defining $\theta_S = (s_x, s_y, D)/\sqrt{s_x^2 + s_y^2 + D^2}$ (as seen in section 2.1), we match the source motion and changes in the parallel projection angle in a coherent way. Changing s from $(0, 0, D)$ to (s_x, s_y, D) will translate any z_1-slice in a manner proportional to the displacement of any z_2-slice undergoing a change of parallel projection from $(0, 0, 1)$ to $(s_x, s_y, D)/\sqrt{s_x^2 + s_y^2 + D^2}$. In the discussion section, we discuss the alternative links between the cone-beam sources and parallel projection angles.

Since the objective is for f_1 and f_2 to have matched cone-beam and parallel projections, we

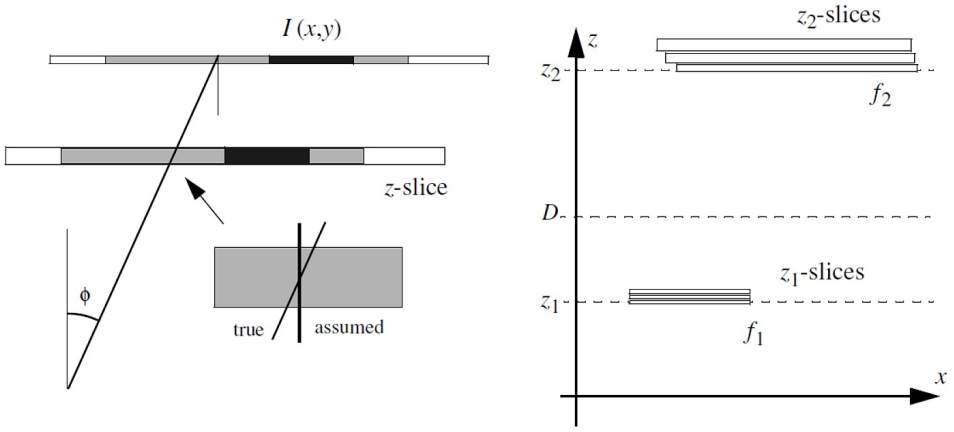

Figure 8: Left: Rays with a non-zero incidence angle ϕ on the detector will have traversed the z-slice obliquely which increases the intensity value recorded on the detector. The true line-length through the z-slice is a factor of $1/\cos\phi$ more than the assumed line-length so the increased intensity factor is also $1/\cos\phi$. Right: The z_2-slices that are used to define f_2 in terms of the z_1-slices of f_1 are thicker than the original z_1-slices, and the thickness varies with z. (This can be seen by imagining a single z_1-slice cut into many smaller slices and tracking where these smaller slices map in the corresponding z_2-slice.) If uncorrected, the thicker z_2-slice will result in increased intensity in the projection $I_2(x, y)$ due to the longer path-length travelled by integration rays. (The figure is schematic; not to scale.)

would like their images $I_1(x, y)$ and $I_2(x, y)$ to translate identically as the source moves in the plane with the projection direction following it. For a fixed z_1-slice $f_1(x, y, z_1)$, at $s = (0, 0, 0)$ we identified, for corresponding $\theta = (0, 0, 1)$ the z_2-slice $f_2(x, y, z_2)$ defined by $f_2(Mx, My, z_2) = f_1(x, y, z_1)$ (for any z_2). For a unit displacement of s, we note an image displacement "speed" of $1 - M$, and for the corresponding change in θ_S, the image displacement is in the same direction, with magnitude (depending on z_2) of $(D - z_2)/D$. To find the z_2 slice whose displacement exactly matches a given z_1 slice, we set $(D - z_2)/D = 1 - M$ and solve for z_2. Recalling that $M = D/z_1$, we obtain $z_2 = D^2/z_1 = DM$. In summary, to match magnification and translation effects, we define the z_2-slices of f_2 in terms of the given z_1-slices of f_1 as $f_2(Mx, My, MD) = f_1(x, y, z_1)$.

We note that if the z_1-slice is behind the detector ($z_1 > D$) then the z_2 slice will be in front of the detector ($z_2 < D$) resulting in both images I_1 and I_2 moving in the same direction as the source movement. It is again easily seen using a new diagram (not shown) that for $z_2 < D$ the movement of $I_2(x, y)$ on the detector is still $(D - z_2)/D$ in response to a unit change of projection direction θ.

The other two physical effects are essentially touch-ups. The main principle, as described above, is to position and scale the z_2-slice so that $I_2(x, y)$ matches the image $I_1(x, y)$ of the z_1-slice, for all positions of the cone-beam source.

3.3 The cosine of the incidence angle

The role of the leading "cosine term" in front of the integrals in equations (1) and (3) is to compensate the effect of oblique rays traversing the thin z-slice. The normal vector to all the z-slices is $(0, 0, 1)$ and we define the angle of incidence ϕ as the angle between this normal vector and the integration direction along the ray in equations (1) and (3). It is easily verified that $\cos\phi$ is the leading term of those equations, so each ray-sum is scaled by $\cos\phi$ when defining the (cosine-weighted) projections. Figure 8 (left) shows that any ray with non-zero incidence angle will contribute a larger intensity to the image $I(x, y)$ by a factor of $1/\cos\phi$ if not corrected. The cosine correction ensures that the image does not change intensity when translated on the detector due to moving source locations or to new parallel projection angles.

3.4 The varying thickness of the thin slices

The last part of the formulas to be explained is the weighting term of D^2/z^2 in equation (5). This factor arises from the changing thickness of the z_2-slices. We start with all z_1-slices having the same thickness (say Δ, which is presumed small), but the z_2-slices will all have different thicknesses, which depend on the location of the corresponding z_1-slices, see figure 8 (right). These increased thicknesses will increase the intensity levels of the projections $I_2(x, y)$ unless they are compensated appropriately. To compensate, we must find the z_2-slice thicknesses. They are straight-forwardly seen to be Δ times D^2/z_1^2 where z_1 is the location of the corresponding z_1-slice. This formula is obtained (for example) by taking differentials: starting from the positioning formula given above, $z_2 = D^2/z_1$, we obtain $dz_2 = -D^2/z_1^2 dz_1$. (The negative sign just reflects the fact that the z_1-slices and z_2-slices both approach the detector, and thus travel in opposite directions.) To compensate the thicker z_2-slice, the intensity of f_2 needs to be reduced accordingly, so $f_2 = (z_1^2/D^2)f_1 = (1/M^2)f_1$. This decrease in intensity is clearly visible in figure 4 (middle). We note here that if the z_1 slice is on the far side of the detector ($z_1 > D$), the same behavior arises except that now the z_2-slices (which are on the near side of the detector) will be thinner, and the intensity "reduction" (actually an increase in this case) is still according to the formula $f_2 = (1/M^2)f_1$.

3.5 Creating the parallel object f_2 from the cone-beam object f_1 and vice versa

Combining this final result with the previous formula we see that the z_1-slice $f_1(x, y, z_1)$ and the corresponding z_2-slice $f_2(x, y, z_2)$ will have the same projections $I(x, y)$ on the detector if f_2 is defined by $M^2 f_2(Mx, My, MD) = f_1(x, y, z_1)$. From a given object function f_1, the corresponding object function f_2 is constructed slice-by-slice according to this formula $\mathcal{T} f_2 = f_1$, which agrees with the definition of equation (5). All 4 features in the formula have been explained physically in the tomosynthesis context. Specifically, the matched "translation speed" of the tomosynthesis image requires $z_2 = MD$, and the cone-beam magnification effect generates a scaling of the parallel-image resulting in $x_2 = Mx$, $y_2 = My$. The change in slice thickness generates the leading term M^2. Finally, the obliquely angled line-integrals are compensated by the "cosine" weighting terms in the integrals of equations (1) and (3).

We now use the same approach for the reverse procedure of constructing a matching cone-beam object f_1 from a given parallel object f_2. The parallel object is conceptually composed of contiguous thin "z_2-slices" of equal thickness. For our geometric description, the parallel object f_2 will lie on the far size of the detector ($z > D$). However the parallel object is assumed to lie anywhere above the x-y plane, and the formulas will still apply.

We first examine the translation speed of the parallel beam projection $I_2(x, y)$ of one of the slices, at $z = z_2$, in response to a change in the tangent of the projection angle. The situation is the same as described in section 3.2, and figure 7 still applies; a unit change in the tangent of the direction vector will generate a shift of $(D - z_2)/D$ of the image $I_2(x, y)$. Similarly, from figure 6, the image $I_1(x, y)$ of the cone-beam projection of a z_1-slice will translate by $(z_1 - D)/z_1$ in response to a unit shift of the x-ray source. Equating these two quantities will identify the location of the z_1-slice of the cone-beam object f_1 that corresponds to a z_2-slice of the parallel object. Solving for z_1 in $(D - z_2)/D = (z_1 - D)/z_1$ results in $z_1 = D^2/z_2$.

The cone-beam magnification of the z_1-slice, as visualized in figure 5, still has the magnitude $M = D/z_1$ so the "width" of the z_1-slice must be reduced (multiplied by $1/M$) for the size of I_1 to match the given parallel projection I_2. The same cosine factors apply as described in figure 8 (left) and these factors are already included in the definitions of the cone-beam and parallel projections. Finally, the variable thickness of the cone-beam slices, due to the uneven spacing (i.e. thickness) of the z_1 slices in response to evenly-spaced z_2-slices, requires an intensity adjustment. The thickness dz_1 of the slice at $z = z_1$, in terms of the parallel slice thickness dz_2 is given by $dz_1 = (D^2/z_2^2)dz_2$ (where again we have taken the absolute value of the derivative for this Jacobian calculation).

Assembling these components, we find that from a given z_2 slice, the corresponding (cone-beam) z_1 slice is defined by $(D^2/z_2^2) f_1(x/M, y/M, D^2/z_2) = f_2(x, y, z_2)$. If we now define $M_2 = 1/M = z_1/D$ and substitute $z_1 = D^2/z_2$ to obtain $M_2 = D/z_2$, our formula then becomes $M_2^2\, f_1(M_2\, x, M_2\, y, M_2\, D) = f_2(x, y, z_2)$. We now note that, given the parallel object f_2, the corresponding cone-beam object f_1, built slice-by-slice, satisfies the formula $\mathcal{T} f_1 = f_2$. Remarkably, this formula is the same as the reverse case (finding a parallel object, in terms of a cone-beam object) $f_2 = \mathcal{T} f_1$ as shown in the first paragraph of this section. The fact that $f_1 = \mathcal{T} f_2$ and $f_2 = \mathcal{T} f_1$ is the reason the transformations are reflections of each other, with the $z = D$ plane being the 'mirror', i.e., the location where the z_2 and z_1 slices are identical.

This reflectivity property is the key to obtaining D-symmetric objects, and arises from the symmetry in the formula $z_1 = D^2/z_2$, i.e. that z_1 and z_2 can be interchanged without affecting the formula. The magic appears here. In the approach used by Edholm and coworkers in the 1990s, this reflectivity property was not present. We return to this point in the discussion section below.

4 Discussion and conclusions

4.1 The Edholm version

The underlying mechanisms of the matched cone-beam and parallel projections were described in the original publications by Edholm and co-workers (Carlsson *et al* 1994) and (Edholm and Danielsson 1996). However, their formulation did not produce the magical reflection property needed. We briefly summarize their approach using the notation of this paper, in order to clarify this point. We use a superscript "E" to indicate the Edholm formulation. Most importantly, we note that the sources lie on the plane $z = D$, and the detector is the plane $z = 0$ which is the reverse of the situation described in this article. Edholm showed that $\mathcal{D}_S^E = \mathcal{P}_{\theta_s}^E \mathcal{T}_{D\to P}^E$, meaning that a certain transform $\mathcal{T}_{D\to P}^E f$ of a "divergent object" f, produces a "parallel object" which has the same parallel projections as the divergent projections of the divergent object.

More precisely, for an object between the source plane and the detector, and source locations $s = (s_x, s_y, D)$, divergent projections are defined by

$$\mathcal{D}_S^E f(u,v) = \int_0^D f(u + \frac{z(s_x - u)}{D}, v + \frac{z(s_y - v)}{D}, z)\, dz \tag{7}$$

and parallel projections are defined by

$$\mathcal{P}_\theta^E f(u,v) = |\theta_z| \int_{-\infty}^{\infty} f(u + t\theta_x, v + t\theta_y, t\theta_z)\, dt. \tag{8}$$

Edholm links parallel projection directions to divergent projection source positions by $\theta_s = s/||s|| = (s_x, s_y, D)/||s||$. In this case, the conversion operator, to convert a divergent object f to a parallel object $\mathcal{T}_{D\to P}^E f$ is

$$\mathcal{T}_{D\to P}^E f(x,y,z) = \begin{cases} Q^2 f(Qx, Qy, Qz) & \text{if } z > 0 \\ 0 & \text{if } z \le 0 \end{cases}, \qquad Q = \frac{D}{D+z} \tag{9}$$

In equation (9), the compact support of (the divergent object) f is assumed to lie between the planes $z = 0$ and $z = D$, which corresponds physically to the object lying between the detector and the plane of the x-ray sources. It can be verified that the corresponding (parallel) object $\mathcal{T}_{D\to P}^E f$ remains above the plane $z = 0$ but with no bound on its extent in z, thus the parallel object also lies between the detector and the "source plane" (which is "at infinity" for the parallel projections).

It is straightforward to demonstrate the Edholm result $\mathcal{P}_{\theta_s}^E \mathcal{T}_{D\to P}^E = \mathcal{D}_S^E$:

$$\begin{aligned} \mathcal{P}_{\theta_s}^E \mathcal{T}_{D\to P}^E f(u,v) &= \frac{D}{||s||} \int_{-\infty}^{\infty} \mathcal{T}_{D\to P}^E f(u + t\frac{s_x}{||s||}, v + t\frac{s_y}{||s||}, t\frac{D}{||s||})\, dt \\ &= \int_0^{\infty} \mathcal{T}_{D\to P}^E f(u + \frac{zs_x}{D}, v + \frac{zs_y}{D}, z)\, dz \\ &= \int_0^{\infty} Q^2 f(Qu + \frac{Qzs_x}{D}, Qv + \frac{Qzs_y}{D}, Qz)\, dz \qquad \text{where } Q = \frac{D}{D+z} \end{aligned}$$

$$
\begin{aligned}
&= \int_0^D f(\frac{(D-z')u}{D} + \frac{z's_x}{D}, \frac{(D-z')v}{D} + \frac{z's_y}{D}, z')\, dz' \\
&= \int_0^D f(u + \frac{z(s_x-u)}{D}, v + \frac{z(s_y-v)}{D}, z)\, dz \\
&= \mathcal{D}_S^E f(u,v) \qquad (10)
\end{aligned}
$$

which validates equation (9) as the correct transformation, and proves the main result of Edholm: $\mathcal{P}_{\theta_s}^E \mathcal{T}_{D\to P}^E = \mathcal{D}_S^E$.

Setting $x' = Qx, y' = Qy, z' = Qz$ in equation (9), it is straightforward to verify that the inverse of $\mathcal{T}_{D\to P}^E$ is $\mathcal{T}_{P\to D}^E$, given by

$$
\mathcal{T}_{P\to D}^E f(x',y',z') = {Q'}^2 f(Q'x', Q'y', Q'z'), \qquad Q' = \frac{D}{D-z'}, \quad 0 < z' < D \qquad (11)
$$

Consequently, we have both $\mathcal{P}_{\theta_s}^E \mathcal{T}_{D\to P}^E = \mathcal{D}_S^E$ and $\mathcal{D}_S^E \mathcal{T}_{P\to D}^E = \mathcal{P}_{\theta_s}^E$. We observe from equations (9) and (11) that $\mathcal{T}_{D\to P}^E f$ and $\mathcal{T}_{P\to D}^E f$ are, in general, different functions, so the roles of the "parallel object" f_P, whose parallel projections match the divergent projections of the "divergent object" f_D, cannot be reversed. Mathematically, if $f_P = \mathcal{T}_{D\to P}^E f_D$ then unlike the situation in section 2, we do not obtain $f_D = \mathcal{T}_{P\to D}^E f_P$. It is this absent property in the Edholm framework that precludes the existence of self-matching objects, such as the D-symmetric object functions.

Although the Edholm formulation does not accommodate the D-symmetry property, we note the more convenient property that, for example, the divergent object lies between $z = 0$ and $z = D/2$ if and only if the parallel object lies between $z = 0$ and $z = D$.

4.2 D-symmetry in the Edholm geometry

In the previous section, we noted that the Edholm formulation did not admit D-symmetric object functions. However, it is straightforward to reformulate the D-symmetry situation described in section 2 into the Edholm geometry of sources on the plane $z = D$ and the detector being the x-y plane. A reflection of the coordinate axes in the plane $z = D/2$ achieves this reformulation, and D-symmetry will then be present in the Edholm geometry.

The vital feature that generates D-symmetry is the correspondence chosen between parallel directions θ and source locations s. Reflecting the axes about $z = D/2$ results in a new correspondence $\bar{\theta}_S = (s_x, s_y, -D)/||s||$, and both the parallel and divergent objects are constrained to lie below the source plane $z = D$. In this case, the mapping from divergent objects to parallel objects, denoted $\mathcal{T}^E$, is defined by

$$
\mathcal{T}^E f(x,y,z) = \begin{cases} \dfrac{D^2}{(D-z)^2}\, f\left(\dfrac{Dx}{D-z}, \dfrac{Dy}{D-z}, \dfrac{-Dz}{D-z}\right) & \text{if } z < D \\ 0 & \text{if } z \geq D \end{cases} \qquad (12)
$$

We now verify that $\mathcal{P}_{\bar{\theta}_s}^E \mathcal{T}^E f = \mathcal{D}_S^E f$, where $\mathcal{D}_S^E$ and $\mathcal{P}_\theta^E$ are still defined using equations (7)

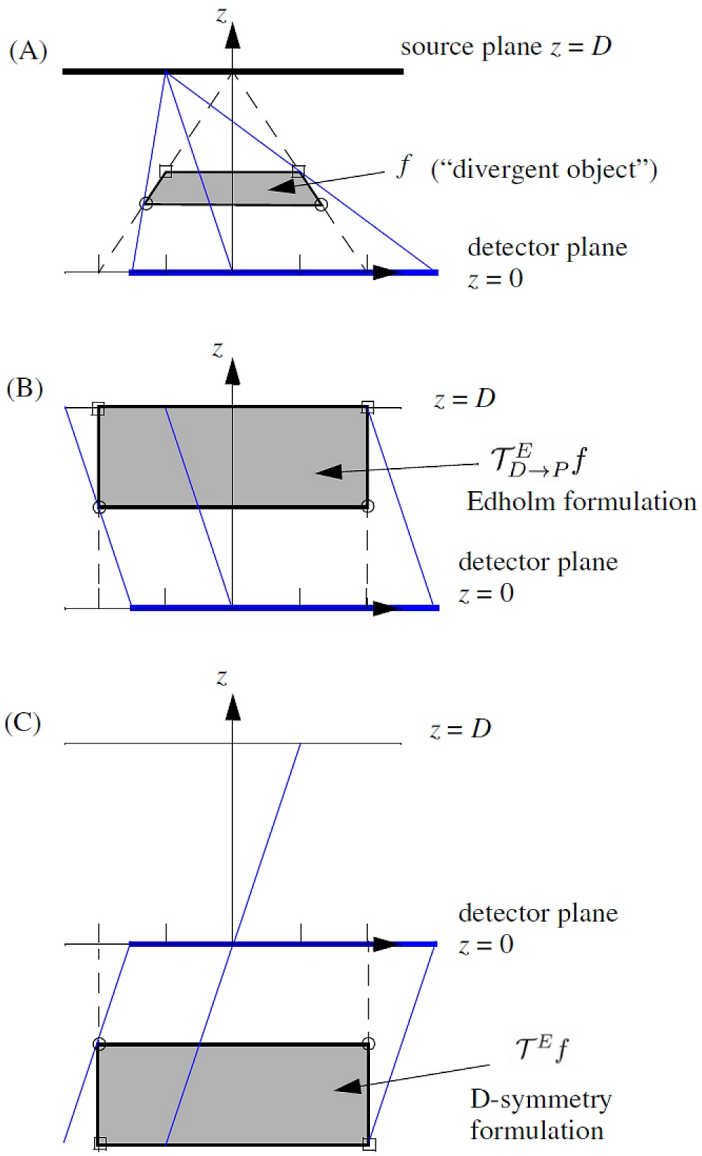

Figure 9: The Edholm geometry. (A) An example "divergent object" f with dotted lines and blue lines showing two divergent projections. (B) A sketch of the "parallel object" $\mathcal{T}^E_{D\to P} f$ according to the Edholm formulation. The two parallel projections corresponding to the divergent projections in (A) are shown. (C) A sketch of the D-symmetric "parallel object" $\mathcal{T}^E f$ presented in the Edholm geometry. The object is on the opposite side (below) the detector. The parallel projection direction is defined differently than for the Edholm formulation in (B), but the two parallel projections of $\mathcal{T}^E f$ still produce the same projections as the divergent projections in (A).

and (8), and $\bar{\theta}_S = (s_x, s_y, -D)/||s||$.

$$\begin{aligned}
\mathcal{P}^E_{\bar{\theta}_s}\,\mathcal{T}^E f(u,v) &= \frac{D}{||s||}\int_{-\infty}^{\infty} \mathcal{T}^E f(u + t\frac{s_x}{||s||}, v + t\frac{s_y}{||s||}, -t\frac{D}{||s||})\,dt \\
&= \int_{-\infty}^{\infty} \mathcal{T}^E f(u - z\frac{s_x}{D}, v - z\frac{s_y}{D}, z)\,dz \\
&= \int_{-\infty}^{D} \frac{D^2}{(D-z)^2} f(\frac{D}{D-z}(u - \frac{zs_x}{D}), \frac{D}{D-z}(v - \frac{zs_y}{D}), \frac{-Dz}{D-z})\,dz \\
&= -\int_{D}^{-\infty} f(\frac{D-z'}{D}u + \frac{z's_x}{D}, \frac{D-z'}{D}v + \frac{z's_y}{D}, z')\,dz' \\
&= \int_{-\infty}^{D} f(u + \frac{z(s_x-u)}{D}, v + \frac{z(s_y-v)}{D}, z)\,dz \\
&= \mathcal{D}^E_S f(u,v). \qquad (13)
\end{aligned}$$

A simple direct calculation using equation (12) shows that $\mathcal{T}^E\mathcal{T}^E f = f$, and therefore $\mathcal{P}^E_{\bar{\theta}_s}\mathcal{T}^E = \mathcal{D}^E_S$ if and only if $\mathcal{P}^E_{\bar{\theta}_s} = \mathcal{D}^E_S\mathcal{T}^E$. D-symmetry in this Edholm system is defined by $\mathcal{T}^E g = g$. We thus obtain, as before, matched parallel and divergent projections, $\mathcal{P}^E_{\bar{\theta}_s} g = \mathcal{D}^E_S g$, for any D-symmetric object g.

Figure 9 illustrates these two situations in the Edholm geometry: the Edholm formulation uses $\theta_S = s/||s||$, and D-symmetry arises if $\bar{\theta}_S = (s_x, s_y, -D)/||s||$ instead. It also emphasizes other features of these two cases.

In the original Edholm formulation ($\theta_S = s/||s||$), both the parallel and divergent objects are always above the detector plane, and additionally the divergent object is always below the source plane. For the D-symmetry formulation, it is not possible to have both objects on the same side of the detector so necessarily, one object will lie at least partially on the other side (i.e. below the detector).

Another feature concerns the correspondence between source locations and parallel directions. In general, given any divergent projection and any parallel projection, there will always be exactly one ray in common to both projections. For source locations on the z-axis, such as $s = (0, 0, D)$, the parallel projection $\theta = (0, 0, 1)$ has the z-axis as the common ray, and in both the Edholm geometry and the original geometry of sections 2 and 3, this common ray strikes the center of the detector. In the Edholm context, with $\theta_S = s/||s||$, the common ray always strikes the center of the detector, no matter what source position is chosen on the source plane. However, for the D-symmetry case ($\bar{\theta}_S = (s_x, s_y, -D)/||s||$), only the source position $s = (0, 0, D)$ will have the common ray strike the middle of the detector (at the origin). All other source positions result in the common ray being more and more oblique, intersecting the detector further and further from the origin. In this sense, the Edholm correspondence $\theta_S = s/||s||$ is more natural than the D-symmetry correspondence.

So, although the Edholm formulation does not have the D-symmetry property, it has a more natural correspondence between the parallel and divergent projections, and the more satisfactory situation of both the parallel and divergent objects lying on the same side of the detector.

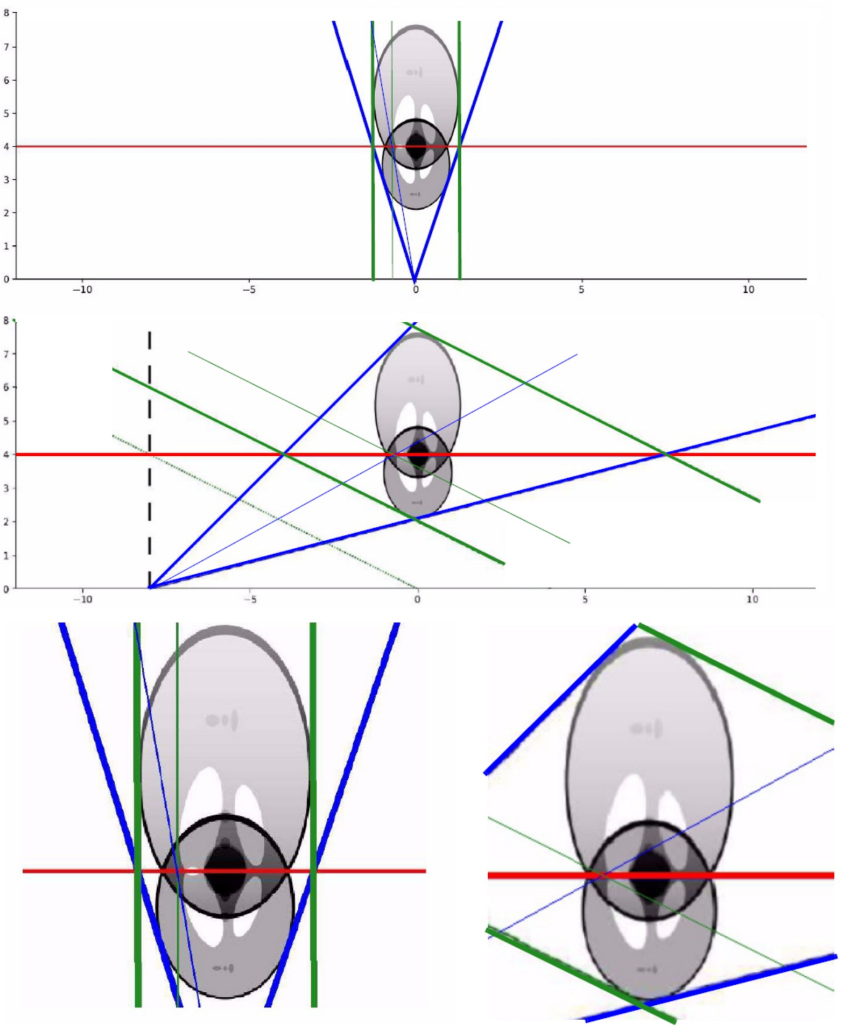

Figure 10: Illustration of the mechanism of matched projections. Top: One line (one element) from each of the parallel and divergent projections at $s = (0, 0), \theta_s = (0, 1)$ is considered. The thin green and blue lines intersect at the detector, so their integrated values should be equal. Middle: Same as top figure, except $s = (-8, 0), \theta_s = (-8, 4)/4\sqrt{5}$. Bottom left: Magnified view of top figure, illustrating that the thin green line traverses the same features of the object as does the thin blue line. Bottom right: Same as bottom left, for the case shown in the middle figure.

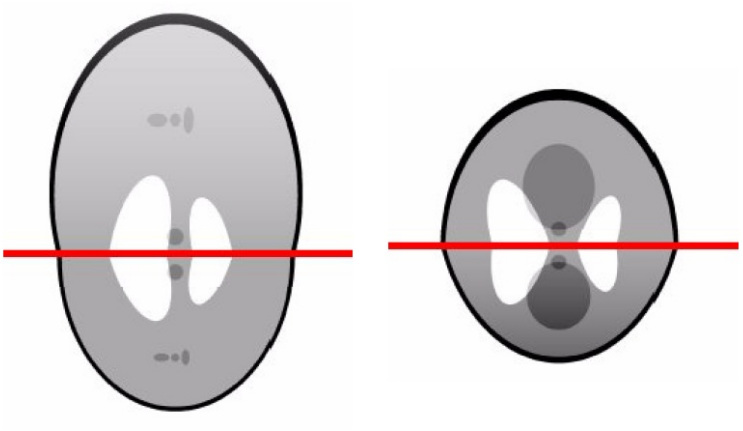

Figure 11: Two further examples of D-symmetric functions that can be generated by translating and truncating the Shepp-Logan phantom at the detector, before adding the D-reflection.

4.3 Further illustrations

As a complement to figure 3, figure 10, top shows the same D-symmetric object function, but this time the projections at $s = (0, 0, 0)$ and $\theta_s = (0, 0, 1)$ are indicated. There are two thin projection lines shown, intersecting the virtual detector at roughly $(-0.7, D)$ (with $D = 4$), and a magnified view is presented bottom left. The figure is intended to illustrate the mechanism of the self-matching property of D-symmetric functions. The thin green and blue lines intersect each other at the detector, which is shown as a thick red horizontal line. The green and blue lines are respectively single values of the parallel and divergent projections. The two identical detector measurements are the integrated density over the thin vertical green line, and the integral over the thin blue line (for the source at the origin). Looking closely, the segment of green line below the detector integrates over object density features identical to those of the blue line above the detector, and vice versa for the rest of the green line (above the detector) and the rest of the blue line (below the detector). This behavior explains why the integrated values for these two lines are equal to each other, and is directly attributed to the D-symmetric nature of the object. Although not shown in the figure, this same behavior occurs for *all* green-blue pairs for this vertical parallel projection and the divergent projection with source at the origin. Furthermore, and much more striking, for any oblique parallel projection and corresponding divergent projection, the same behavior can be observed for this D-symmetric function. Figure 10 (middle) shows, for the same object, a second projection direction with the source at $(-8, 0)$ and one pair of rays intersecting on the detector. Again, the features traversed by the thin green and blue lines are the same due to the D-symmetry of the object; see figure 10 (bottom right).

The example D-symmetric function of figures 3 and 10 was chosen to emphasize the possibility of an overlapping construction of the function. More reasonable-looking D-symmetric objects can be obtained by first truncating at the $z = D$ line before reflecting. Figure 11 shows two such examples, also obtained from a truncated Shepp-Logan phantom.

The example of figure 11 (left), was constructed by taking the bottom half of the Shepp-Logan phantom (see figure 4 (top)) and translating it vertically, to be 'hanging' from the red detector line. The D-reflection was then computed and added to form the D-symmetric object shown in the figure. Note that the background intensity level in the bottom half of the object is constant, whereas in the top half it decreases with increasing distance from the detector, as expected.

The example of figure 11 (right) was constructed similarly, but this time by taking slightly less than the top half of the Shepp-Logan phantom, and translating it vertically to be 'sitting' on the detector. After adding the D-reflection we note that the lower half of the phantom has increasing background intensity with increased distance (lower and lower) from the detector.

4.4 Significance of the D-symmetry concept

No imaging applications of D-symmetric object functions are described here, and consequently the results of this article could just be considered as a curiosity. However, they are unexpected and counter-intuitive, and therefore provide substantial new information on the nature of divergent and parallel projections.

In addition to furthering our understanding of image reconstruction theory, these results provide a warning in some applications contexts. In particular, range conditions of projection operators, also known as data consistency conditions (DCC) are finding a broad range of applications. The basic idea is that projection data usually have some inherent redundancy, known as the DCC, which can be invoked to extract parameters of some systematic effect not modelled in the projections.

One example would be to use DCC to find geometric calibration parameters of a scanner; the projections are first used to determine the scanner geometry, and then used for image reconstruction in a second step. Implicit in this DCC approach is the notion that if all the DCC are satisfied, then the correct parameters have been identified because projections are assumed to correspond uniquely to the object that was scanned and equivalently, the scanner geometry is uniquely determined. But already from Edholm's result (equation (10)), we know that different objects can match the (DCC-compatible) projections if the scanner geometry is unknown. The D-symmetry concept presented in this article goes a step further and shows that even if some *a priori* knowledge of the object is applied, the projections still do not necessarily identify the scanning geometry (divergent or parallel). As a specific example, a geometric calibration procedure using a *known* calibration phantom (i.e., with *full* knowledge) would not be able to distinguish a parallel system from divergent if the phantom were (close to) D-symmetric for some D. Phantoms made up of a collection of isolated point objects might be unknowingly close to D-symmetric.

4.5 Summary

We have defined the notion of D-symmetric object functions, and described a simple procedure to obtain many such functions. The main result of this article is that D-symmetric functions have the remarkable property that every parallel projection of a D-symmetric object is identical to a certain divergent projection (fanbeam or cone-beam in two- or three-dimensions) of the same

object. As well as a straight-forward mathematical proof of this result, we also provided a detailed physics-style demonstration in the context of classical linear tomosynthesis.

The foundation of this result is a transformation originally published by Edholm and co-workers that provides a "parallel object" f_P from a "cone-beam object" f_D. The parallel projections of f_P match the cone-beam projections of f_D. In their formulation of the geometry however, the detector was the x-y plane and the cone-beam sources lay on a parallel plane. In this Edholm geometry, a different transformation was required to convert cone-beam objects into parallel objects. In a different geometric formulation, proposed by Defrise, the sources lie on the x-y plane and the detector is on the parallel plane $z = D$. The correspondence between source locations and the directions of the parallel projections was also different. In the Defrise formulation, the transformation that maps f_P to f_D is the *same* as the reverse mapping from f_D to f_P. When this magical transformation is used to define D-symmetry, the "self-matching" property of D-symmetric functions arises, whereby their cone-beam and parallel projections all match.

Although no imaging applications of D-symmetric functions have been described, we indicated that the existence of such counter-intuitive anomalies can provide a warning in contexts such as applications that invoke data consistency conditions. Also, the concepts presented in the physical description of section 3 are directly relevant for linear tomosynthesis, and might be instructive in this imaging context.

Acknowledgments

This work was partially supported by grants ANR-17-CE19-0006 (ROIdor project) and ANR-21-CE45-0026 (SPECT-Motion-eDCC) from the Agence Nationale de la Recherche, France.

References

[Bou18] T. Boulier, R. Clackdoyle, J. Lesaint, L. Desbat (2018) Consistency of fan-beam projections of a translating object along an arc of a circle *The Fifth International Conference on Image Formation in X-Ray Computed Tomography, Salt Lake City, USA. May 20-23, 2018* pp. 114–118.

[Buz08] T. M. Buzug (2008) *Computed Tomography. From Photon Statistics to Modern Cone-Beam CT* Springer, Berlin Heidelburg

[Car94] P. E. Carlsson, P. R. Edholm, and P.-E. Danielsson (1994) The synthesis of a new x-ray picture identical in projection to a previous picture using 3D Fourier techniques. *Phys. Med. Biol.* 39:597–608.

[Cla13a] R. Clackdoyle (2013) Necessary and Sufficient Consistency Conditions for Fanbeam Projections along a Line. *IEEE Trans. Nuc. Sci.* 60:1560–1569.

[Cla13b] R. Clackdoyle and L. Desbat (2013) Full data consistency conditions for cone-beam projections with sources on a line *Phys. Med. Biol.* 58:8437–8456.

[Cla14] R. Clackdoyle, S. Rit, J. Hoskovec, L. Desbat (2014) Fanbeam Data Consistency Conditions for Applications to Motion Detection *The 3rd International Conference on Image Formation in X-Ray Computed Tomography, Salt Lake City, USA. June 22-25, 2014* pp. 324–328.

[Cla15a] R. Clackdoyle and L. Desbat (2015) Data consistency conditions for truncated fanbeam and parallel projections *Med. Phys.* 42:831–845.

[Cla15a] R. Clackdoyle, M. Defrise, L. Desbat, J. Nuyts (2015) Consistency of Fanbeam Projections Along an Arc of a Circle *The 13th International Meeting on Fully Three-Dimensional Image Reconstruction in Radiology and Nuclear Medicine, Newport, RI, May 31-June 4, 2015.* pp. 415–419.

[Cla18] R. Clackdoyle (2018) Data Consistency for Linograms and Planograms *IEEE Trans. Rad. Plasma Med. Sci.* 2:288–299.

[Def17] M. Defrise (2017) *Private Communication* (Email from M. Defrise to R. Clackdoyle and L. Desbat sent February 2, 2017, with attachment.)

[Def94] M. Defrise and R. Clack (1994) A cone-beam reconstruction algorithm using shift-variant filtering and cone-beam backprojection *IEEE Trans. Med. Imag.* 13:186–195.

[Des19] L. Desbat and R. Clackdoyle (2019) Calibration and data consistency in parallel and fan-beam geometries *Conference Record of the 2019 IEEE Nuclear Science Symposium and Medical Imaging Conference, Manchester, UK* (4 pages)

[Edh96] P. R. Edholm and P.-E. Danielsson (1996) A theorem on divergent projections. *Three Dimensional Image Reconstruction in Radiology and Nuclear Medicine.* P Grangeat and J L Amans eds (Amsterdam: Kluwer) 35–45.

[Edh98] P. R. Edholm and P.-E. Danielsson (1998) Divergent X-ray projections may under certain conditions be treated as parallel projections. *Comp. Meth. Prog. Biomed.* 57:91–94.

[FDK84] L. A. Feldkamp, L. C. Davis, J. W. Kress (1984) Practical cone-beam algorithm *J. Opt. Soc. Am. A* 1:612–619.

[Joh38] F. John (1938) The ultrahyperbolic equation with 4 independent variables *Duke Math. J.* 300–322.

[Les17] J. Lesaint, S. Rit, R. Clackdoyle, L. Desbat (2017) Calibration for circular cone-beam CT based on consistency conditions *IEEE Trans. Rad. Plasma Med. Sci.* 1:517–526.

[Net07] B. E. Nett, S. Leng, G.-H. Chen (2007) Planar tomosynthesis reconstruction in a parallel-beam framework via virtual object reconstruction *Proc. SPIE Vol 6510* 651028-1–651028-12.

[Ngu20] H. Nguyen, L. Desbat, R. Clackdoyle (2020) Automatic geometric calibration in 3D cone-beam geometry with sources on a line *The 6th International Conference on Image Formation in X-Ray Computed Tomography, Regensburg, Germany (virtual only). August 3-7, 2020* pp. 530–533.

[Pat00] S. K. Patch (2000) Almost-everywhere extrapolation from cone-beam data. US Patent 6,084,936.

[Pat02] S. K. Patch (2002) Computation of Unmeasured Third-Generation VCT Views From Measured Views *IEEE Trans. Med. Imag.* 21:801–813.

[TS96] P. A. Toft and J. A. Sorenson (1996) *The Radon Transform – Theory and Implementation* Kgs. Lyndgby, Denmark: Technical University of Denmark (DTU).

[Zhu07] L. Zhu, S. Yoon, R. Fahrig (2007) A short-scan reconstruction for cone-beam CT using shift-invariant FBP and equal weighting *Med. Phys.* 34:4422–4438.